Virologica Sinica 40 (2025) 535–545

Contents lists available at ScienceDirect

Virologica Sinica

journal homepage: www.keaipublishing.com/en/journals/virologica-sinica
www.virosin.org

Research Article

Epidemiological and genomic surveillance of influenza A virus (pdm09 H1N1 and H3N2) strains from 2017 to 2025 in Tianjin, China

Mingkun Wu [a,b], Liru Guo [a,b], Mei Kong [a,b], Ming Zou [a,b], Xiaochang Liu [a,b], Xiaoyan Li [a,b,c,*]

[a] Institute of Microbiology, Tianjin Centers for Disease Control and Prevention, Tianjin, 300011, China
[b] Tianjin Key Laboratory of Pathogenic Microbiology of Infectious Disease, Centers for Disease Control and Prevention, Tianjin, 300011, China
[c] Key Laboratory of Prevention and Control of Major Diseases in the Population, Ministry of Education, Tianjin Medical University, Tianjin, 300070, China

ARTICLE INFO

Keywords:
Epidemiology
Influenza A virus (IAV)
Next-generation sequencing
Antigenicity
Drug resistance

ABSTRACT

Influenza A virus (IAV) remains a global public health concern, causing influenza-like illness and severe respiratory tract infections. Two major subtypes, A/pdm09 H1N1 and A/H3N2, circulate globally, and their epidemics are influenced by multiple factors, especially during the COVID-19 pandemic. Based on data from the National Influenza Surveillance Program in China, we analyzed the epidemiological and genomic data in Tianjin collected from 2017 to 2025. A total of 77,473 throat swabs were collected, of which 9144 were IAV-positive. The A/pdm09 H1N1 and A/H3N2 lineages exhibited distinct epidemics across different influenza seasons, with a decline in cases observed during the COVID-19 pandemic. We sequenced the genomes of 128 A/pdm09 H1N1 and 113 A/H3N2 clinical isolates and characterized their temporal evolution and genetic diversity using time-scaled phylogenetic analysis. Additionally, we conducted a genetic risk evaluation of the hemagglutinin and neuraminidase segments, identifying key amino acid residues associated with viral adaptation, transmissibility, virulence, and drug resistance. Moreover, no antigenic variants were found in clinical isolates during the recent influenza seasons, though reduced sensitivity to oseltamivir and zanamivir was observed in individual strains. Our surveillance highlights the epidemiology and evolution of IAV before and after the COVID-19 pandemic in Tianjin.

INTRODUCTION

Influenza A virus (IAV) is a recognized major pathogen that causes respiratory tract infections in humans, livestock, and wildlife (Lee et al., 2024). The World Health Organization (WHO) estimates that approximately 5–15% of the global population is infected annually with seasonal influenza viruses, resulting in 3–5 million severe cases and approximately 250,000–650,000 deaths (Zhao et al., 2024). Nearly 99% of deaths in children under 5 years old in developing countries are attributed to influenza-related lower respiratory infections (Nair et al., 2011).

In taxonomy, the IAV belongs to the family *Orthomyxoviridae*, genus *Influenzavirus A* (Krammer et al., 2018). The genome of IAV consists of negative-sense RNA, comprising eight gene segments: the polymerase acidic (PA), the RNA polymerase subunits polymerase basic 2 (PB2), and polymerase subunits polymerase basic 1 (PB1), which together form the viral RNA-dependent RNA polymerase. Additionally, the genome encodes hemagglutinin (HA), neuraminidase (NA), nucleoprotein (NP), matrix proteins (M), and non-structural proteins (NS) (Chon et al., 2024). Among them, HA and NA are the surface glycoproteins of the influenza virus and play critical roles in the virus life cycle (Lee et al., 2018). Hemagglutinin binds to α2,6-linked sialic acids (α2,6-SA) on human upper airway epithelial cells, mediating viral attachment and entry (Chandrasekaran et al., 2008). Neuraminidase cleaves sialic acids (SA) from glycans to facilitate the release of budding progeny virions (Wagner et al., 2002; Lee et al., 2018).

IAVs are further classified into several subtypes based on their HA and NA segments (Gamblin and Skehel, 2010). Two major subtypes of IAV [the 2009 pandemic IAV (A/pdm09 H1N1) and the H3N2 IAV (A/H3N2)] are endemic in human worldwide (Lee et al., 2024; Li et al., 2024). The A/pdm09 H1N1 virus originated in Mexico and the United States in April 2009, leading to a subsequent global pandemic worldwide between June 2009 and August 2010 (Wedde et al., 2015; Xing

* Corresponding author.
E-mail address: xiaoyanli1291@163.com (X. Li).

https://doi.org/10.1016/j.virs.2025.07.011
Received 21 April 2025; Accepted 25 July 2025
Available online 30 July 2025

et al., 2021). The genome of this virus consists of segments from swine, avian, and human lineages resulting from triple reassortment, and it replaced the previously circulating seasonal A/H1N1 viruses (Ye et al., 2010; Jayaraman et al., 2011). The currently circulating seasonal A/H3N2 subtype has been circulating in the human population since 1968 as a reassortant between the previously seasonal A/H2N2 virus and an avian A/H3 virus. This subtype has been reported to cause higher attack rates and more hospitalizations (Zhao et al., 2024). Meanwhile, unusual influenza outbreaks or epidemics that occur in summer in temperate regions have been related to A/H3N2 strain infections (Tsou et al., 2017; Zhao et al., 2024). Apart from these two major lineages in the human population, other avian and mammalian IAVs might overcome species barriers, resulting in interspecies transmission and adaptation (Imai et al., 2012; An et al., 2019).

In the context of One Health and Disease X preparedness following COVID-19, IAV epidemiological surveillance is vital to monitoring pathogens and tracking pandemic threats. The high frequency of mutation in the RNA genome can lead to IAV antigenic drift and shift, which may alter host adaptation, increase transmissibility, and enhance virulence, leading to severe clinical burdens (Nelson et al., 2008; An et al., 2019; Xing et al., 2021). Meanwhile, recent studies have reported mutations in the NA segment that confer resistance to common NA inhibitor (NAI) antiviral drugs such as oseltamivir and zanamivir (Butler et al., 2014; Andreev et al., 2024). Furthermore, potential interspecies transmission might occur due to reassortment events between segments from humans and animal reservoirs such as poultry and swine. Therefore, genomic analysis of circulating IAV strains is essential for effective molecular monitoring and early warning.

In this study, we first retrospectively analyzed IAV epidemiological data collected from October 2017 to March 2025 from the surveillance network in Tianjin, a northern coastal city in China. We then performed phylogenetic analysis on 128 A/pdm09 H1N1 and 113 A/H3N2 clinical isolates using next-generation sequencing. We also conducted risk evaluations focusing on host adaptation, transmissibility, virulence, and drug resistance. In addition, we tested the HA antigenicity and susceptibility to NAI antiviral drugs in A/H3N2 and A/pdm09 H1N1 strains isolated during the epidemic season between 2023 and 2025.

RESULTS

Epidemic patterns of A/pdm09 H1N1 and A/H3N2 viruses in Tianjin, 2017–2025

Based on data from the Tianjin influenza surveillance network, we collected 77,473 throat swabs from patients with influenza-like illness (ILI) or severe acute respiratory infections (SARI) at 21 sentinel hospitals between October 2017 and March 2025 (Supplementary Table S1). This included 73,536 throat swabs from ILI patients and 3937 throat swabs from SARI patients. We detected A/pdm09 H1N1 and A/H3N2 viruses in these samples using real-time qPCR (Fig. 1A).

Among all samples, 9144 tested positive for either A/pdm09 H1N1 virus (n = 4227) or A/H3N2 virus (n = 4917), with 14 samples being

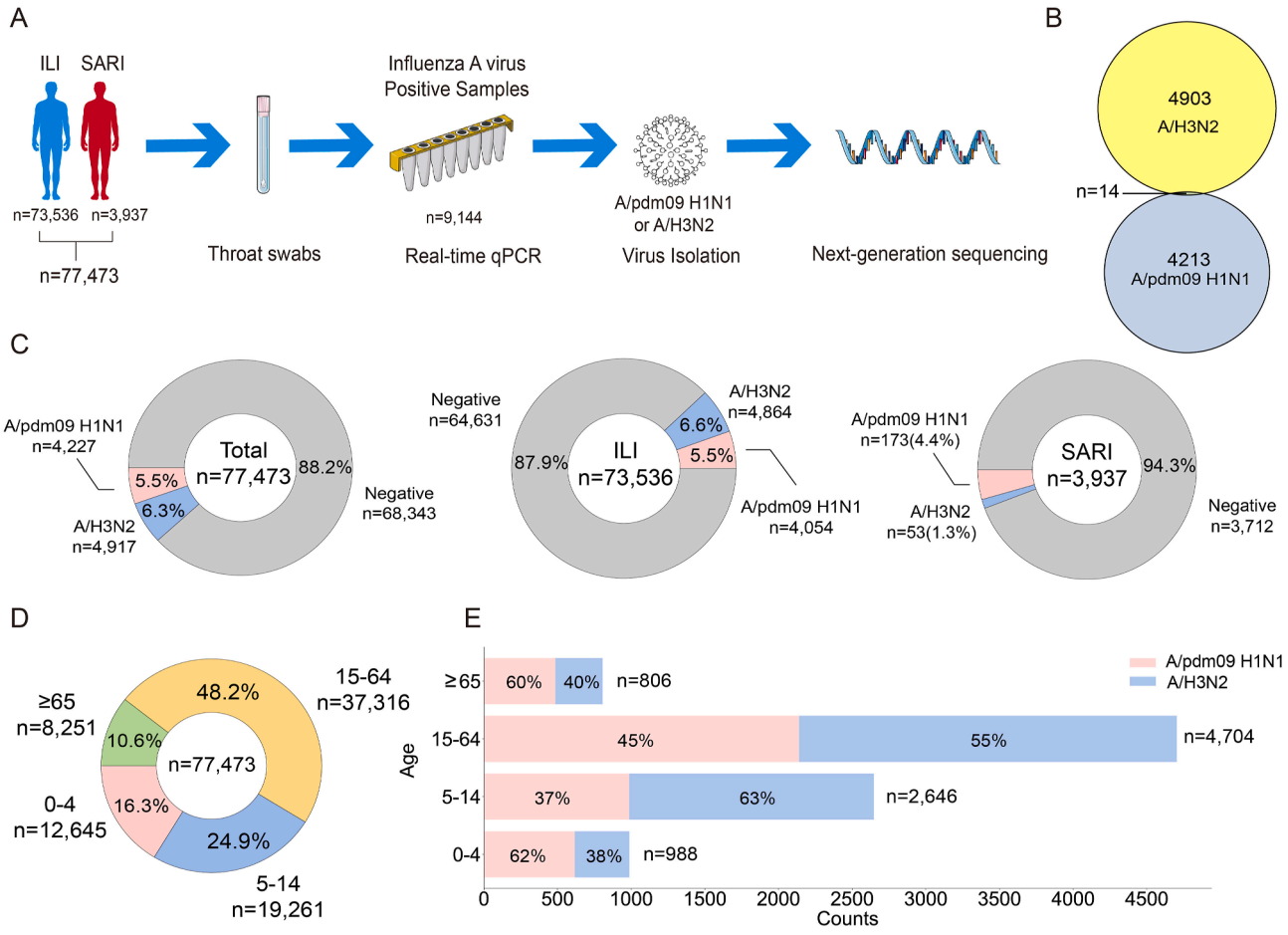

Fig. 1. Epidemic pattern of the influenza A virus in Tianjin between 2017 and 2025.
A. Schematic diagram of study design. **B.** The number of influenza A virus (IAV)-positive samples detected using real-time qPCR. **C.** The ratio of IAV-positive samples detected by real-time qPCR in different populations. **D.** The ratio of samples collected from participants of different ages in this study. **E.** The ratio of A/pdm09 H1N1 and A/H3N2 positivity in IAV-positive patients of different ages. The X-axis refers to the quantity of IAV-positive samples in the real-time qPCR. The Y-axis indicates the age groups. ILI: influenza-like illness. SARI: severe acute respiratory tract infection.

positive for both viruses (Fig. 1B). The overall positive rate was 5.5% (4227/77,473) for A/pdm09 H1N1 virus and 6.3% (4917/77,473) for A/H3N2 virus during the study period (2017–2025) (Fig. 1C). When stratified by patient type, the positive rate for A/pdm09 H1N1 virus was 5.5% (4054/73,536) in ILI patients versus 4.4% (173/3937) in SARI patients. For A/H3N2 virus, the positive rate was 6.6% (4864/73,536) in ILI patients but lower at 1.3% (53/3937) in SARI patients (Fig. 1C).

To examine IAV infection patterns by age, all patients were divided into four groups: infants (0–4 years, n = 12,645), school-aged children (5–14 years, n = 19,261), adults (15–64 years, n = 37,316), and elderly individuals (≥ 65 years, n = 8251) (Fig. 1D). As shown in Fig. 1E, the positive rate for IAV was higher in the school-age group (n = 2,646, 13.7%) and adult group (n = 4,704, 12.6%) compared with the infant group (n = 988, 7.8%) and elderly group (n = 806, 9.8%). Moreover, the proportion of A/pdm09 H1N1 cases was significantly higher than A/H3N2 cases in both the infant group ($\chi^2 = 115.8$, $P < 0.001$) and elderly group ($\chi^2 = 70.40$, $P < 0.001$). Conversely, the proportion of A/pdm09 H1N1 cases was significantly lower than A/H3N2 cases in the school-age group ($\chi^2 = 120.3$, $P < 0.001$). In the adult group, no significant difference was observed between A/pdm09 H1N1 and A/H3N2 cases proportions ($\chi^2 = 2.222$, $P = 0.1360$) (Table 1).

We next analyzed the epidemic characteristics of A/pdm09 H1N1 virus and A/H3N2 virus from 2017 to 2025. With the exception of 2020–2021 and 2021–2022, a distinct peak of IAV infection occurred during winter each year. The A/pdm09 H1N1 subtype predominated during the 2017–2018, 2018–2019, and 2024–2025 epidemic seasons, while the A/H3N2 subtype was dominant in 2019–2020 and 2023–2024 (Fig. 2A). The 2022 winter epidemic season was delayed and featured overlapping peak for both A/pdm09 H1N1 and A/H3N2 subtypes. Notably, another A/H3N2 peak occurred in summer 2022. Similar temporal patterns were observed for both subtypes in ILI and SARI patients (Fig. 2B and C).

Phylogenetic analysis of A/pdm09 H1N1 and A/H3N2 isolates, 2017–2025

We sequenced the genomes of 128 A/pdm09 H1N1 and 113 A/H3N2 clinical isolates and conducted Bayesian evolutionary analysis using sampled trees. The time-scaled phylogeny of the H1 gene showed that all 128 A/pdm09 H1N1 isolates belonged to the 6B.1 lineage. As shown in Fig. 3A, some 2017–2018 strains evolved into the 6B.1A clade, with 2018 strains further differentiating into 6B.1A.1 and 6B.1A.5a clades. The genetic diversity of 2019 strains increased, with isolates representing 6B.1A.1, 6B.1A.4, 6B.1A.5, 6B.1A.6, and 6B.1A.5a clades. Meanwhile, one strain isolated at early 2020 formed the 6B.1A.5a.1 clade, while all post-COVID-19 isolates clustered within the 6B.1A.5a.2a clade. The dominant C.1 subclade in 2023 was subsequently replaced by C.1.9 and C.1.9.3 subclades in 2024–2025.

As shown in Fig. 3B, the A/H3N2 clinical isolates were grouped into diverse branches in the H3 gene phylogenetic tree. During the 2017–2018 epidemic season, we observed 3C.2a1, 3C.2a2, and 3C.2a3 clades. By late 2019 to early 2020, the isolates had diverged into 3C.2a1b.1a and 3C.2a1b.1b clades. After the COVID-19 pandemic, the 3C.2a1b.2a.2a.3a.1 clade emerged as the dominant clade in Tianjin during the annual epidemic season. And different subclades were identified in 2023 (J, J.1, J.2.1, and J.3) and 2024 (J.1, J.2, and J.2.1).

To assess genetic diversity, we analyzed viral evolution and potential reassortment events between HA and NA lineages. For NA lineages in A/pdm09 H1N1 strains (Fig. 3C), A.1 and A.1.1 were predominant in 6B.1 and 6B.1A clades during 2017–2018. Subsequently, B and B.1 lineages emerged in the 6B.1A.5a clade since 2018, with B.1 becoming the dominant lineage in 2019. Moreover, B.2 lineage was detected in the isolate from 2020 (6B.1A.5a.1 clade). All post-COVID-19 strains clustered within the 6B.1A.5a.2a clade, with two prevalent NA lineages (C.5.3 and C.5.3.1). The C.5.3 lineage was exclusively present in the C.1 subclade in 2023, later evolving into C.5.3.1 lineage in C.1.9 and C.1.9.3 subclades during 2024–2025 (Fig. 3A).

For the A/H3N2 subtype, the NA lineage in 3C.2a1, 3C.2a2, and 3C.2a3 clades in 2017–2018 epidemic season included A.1, A.2, and A.2.2 (Fig. 3D). The A.2.2 lineage persisted in 3C.2a1b.1a and 3C.2a1b.1b clades during 2019–2020, with five 3C.2a1b.1b strains developing the A.2.2.1 lineage. For the 3C.2a1b.2a.2a.3a.1 clade, which was dominant after COVID-19, the NA lineages belonged to the B.4 lineage and further diverged into B.4.1 and B.4.3 lineages. This was consistent with global evolutionary trends in recent years. Notably, we also detected A.2 lineage in one post-COVID-19 strain, suggesting a potential reassortment event between HA and NA lineages (Fig. 3D).

Table 1
The results of chi-square tests for A/pdm09 H1N1 and A/H3N2 positive quantity in different age groups.

chi-square tests	Groups	A/pdm09 H1N1 positive	A/H3N2 positive	χ^2	*P*-value
1	0–4	616	372	115.8	<0.0001
	Others	3611	4545		
2	5–14	986	1660	120.3	<0.0001
	Others	3241	3257		
3	15–64	2139	2565	2.222	0.1360
	Others	2088	2352		
4	≥ 65	486	320	70.40	<0.0001
	Others	3741	4597		

Risk evaluation of A/pdm09 H1N1 and A/H3N2 isolates: hemagglutinin (HA) and neuraminidase (NA) gene analysis

To evaluate transmission risk in susceptible populations and pathogenicity, we analyzed human-adaptive mutations, transmissibility markers, receptor-binding properties, and virulence determinants in the HA gene. Key findings from the 128 A/pdm09 H1N1 strains revealed human receptor-binding markers in the HA1 region associated with SAα2,6Gal affinity: Asp225, Pro221, Ser210, Val190, Gly190, Gln172, Asn159, Lys145, and Ala137. Notably, Asn159 was exclusively present in the early isolates before COVID-19, while Gln172 and Gly190 emerged in post-COVID-19 strains. The amino acid residues related to viral transmissibility showed no significant temporal difference. Pro186 remained the predominant residue for host adaptation and virulence throughout the study period. Additionally, several amino acid residues that enhanced virulence were identified across different years, including Glu131, Ser144, Ser198, and Gly225 (Fig. 4A).

As shown in Fig. 4B, we identified specific markers associated with receptor-binding (Ile192), transmissibility (Asp190), and host adaptation (Gly144) in the HA1 region of A/H3N2 strains from the period before COVID-19. For the isolates from 2023 to 2024, four asparagine residues (HA1-94, 145, 159, and 186) and a deletion at HA1-133 enhanced viral binding to human receptors. Val223 in the HA1 region was identified as a unique virulence marker. Furthermore, Asn46 in the HA2 region, which affected host adaptation, was only detected after COVID-19. Other markers showed no significant temporal difference. To investigate regional differences in seasonal influenza prevalence, we also analyzed the amino acid markers related to viral infection, transmission, and virulence in global reference strains from 2017 to 2025 (Supplementary Tables S2 and S3). For A/pdm09 H1N1 strains, we found receptor-binding markers (Asp225, Pro221, Ser210, Lys145, and Ala137) in all years. Asn159 and Gln172 were detected before and after COVID-19, respectively. Pro186, an amino acid residue associated with host adaptation and virulence, was found in global strains from different years. For the A/H3N2 subtype, significant temporal markers were also found in other regions, such as the virulence marker Val223 and receptor-binding sites (Asn159 and Asn186) in the HA1 domain. Therefore, several key functional amino acid residues in our study exhibited similar temporal prevalence patterns in other regional strains.

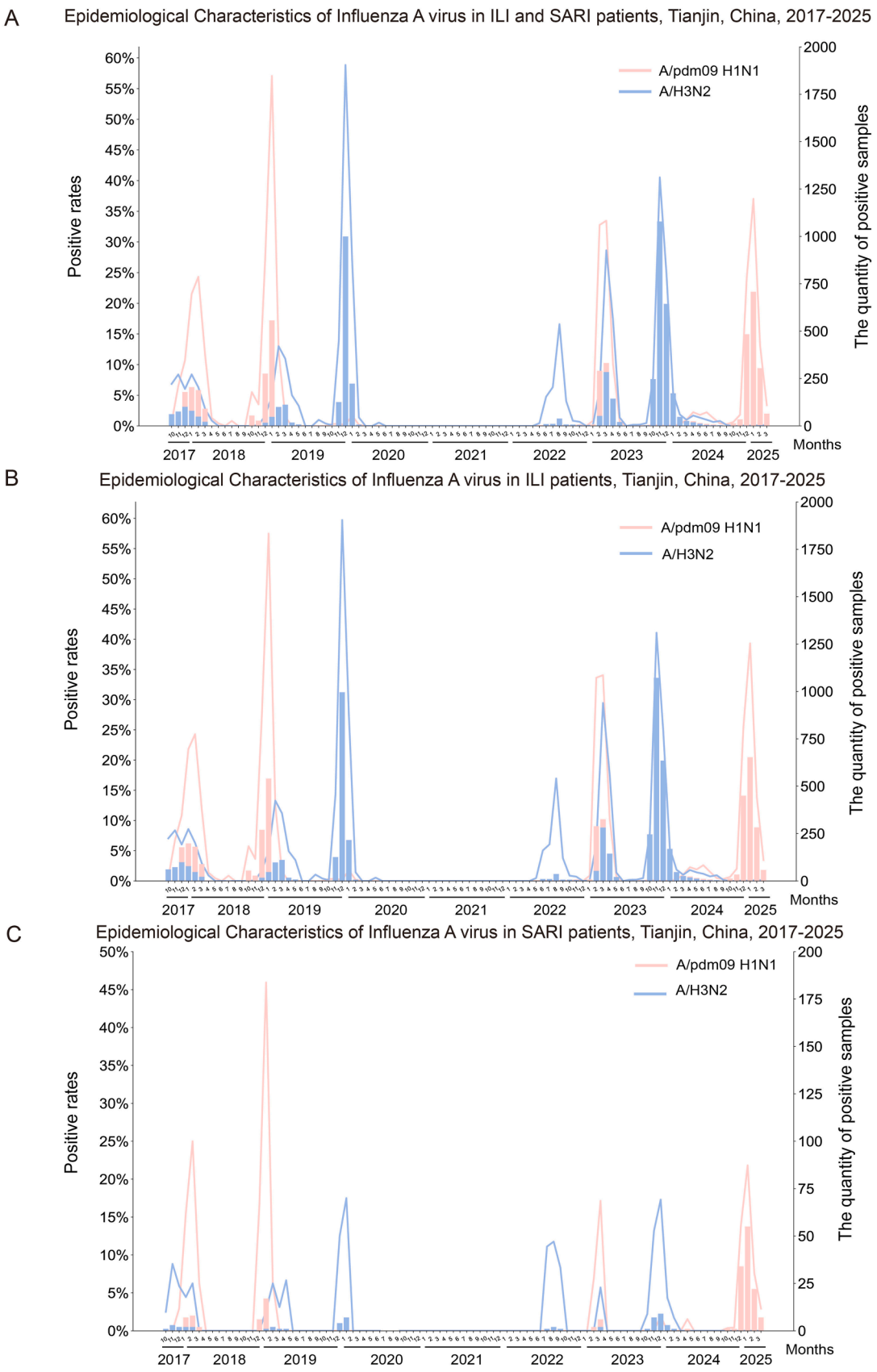

Fig. 2. Epidemiological characteristics of influenza A virus in different patient types in Tianjin, 2017–2025.
The quantity (bar) and positive rates (line) for A/pdm09 H1N1 and A/H3N2 viruses in all (**A**), ILI (**B**), and SARI (**C**) patients from 2017 to 2025 in Tianjin. The X-axis indicates the months. The left Y-axis indicates the positive rates. The right Y-axis refers to the number of positive samples. ILI: influenza-like illness. SARI: severe acute respiratory tract infection.

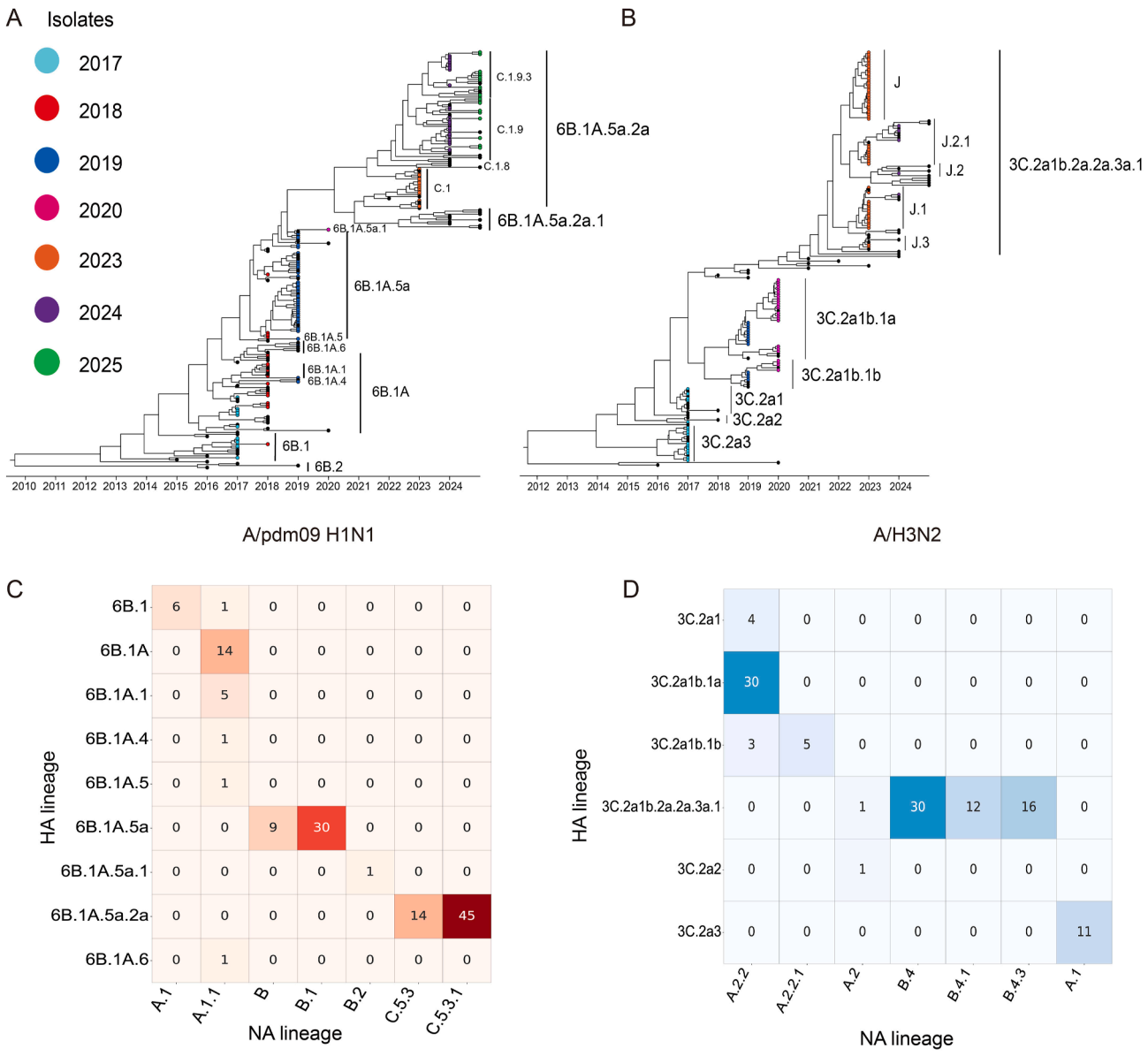

Fig. 3. Phylogenetic analyses for A/pdm09 H1N1 and A/H3N2 subtypes.
A–B. Time-scaled phylogenetic trees based on HA genes for A/pdm09 H1N1 subtype (**A**) and A/H3N2 subtype (**B**). The isolates in this study were labeled with different colors according to date. The reference strains downloaded from the BLAST and GISAID databases were shown in black. Phylogenetic analyses employed a random starting tree with the GTR nucleotide substitution model incorporating estimated base frequencies. The lineage was labeled and annotated using NextClade v3.10.0. **C–D.** The HA and NA lineages in A/pdm09 H1N1 (**C**) and A/H3N2 strains (**D**). The X-axis refers to the NA lineage for A/pdm09 H1N1 (**C**) and A/H3N2 (**D**). The Y-axis refers to HA lineage for A/pdm09 H1N1 (**C**) and A/H3N2 (**D**). The subclades were annotated using Nextclade v3.10.0. The number indicates the quantity of strains for each lineage.

Resistance to common NAI antiviral drugs such as oseltamivir and zanamivir has been widely reported (Butler et al., 2014; Andreev et al., 2024). Therefore, we further analyzed NAI resistance-associated markers in the NA segment. As shown in Fig. 4C and D, the Asp151 substitution, which significantly reduces sensitivity to zanamivir (Boivin, 2013), was detected annually in A/pdm09 H1N1 and A/H3N2 strains. This site exhibited global prevalence in A/pdm09 H1N1 and A/H3N2 clades from 2017 to 2025 (Supplementary Tables S2 and S3). The Tyr274 and Asn246 substitutions, which are other community-acquired mutations (Boltz et al., 2010; Chon et al., 2024), were associated with highly reduced susceptibility to oseltamivir in the A/pdm09 H1N1 subtype. These mutations have also been detected in Tianjin in recent years. In the A/H3N2 subtype, the Asn463, Ala313, and Asn151 substitutions conferred intermediate resistance to NAI drugs. These mutations were mainly detected in 2017, but Asn463 and Ala313 reappeared after COVID-19.

HA antigenicity and resistance to NAI antiviral drugs in A/H3N2 and A/pdm09 H1N1 strains

We further analyzed the HA antigenicity and NAI resistance of influenza A virus. During influenza epidemic seasons after COVID-19, we selected dominant subtypes for analysis, including 21 A/H3N2 strains from 2023 to 2024 and 41 A/pdm09 H1N1 strains from 2024 to 2025. We first detected the reactivity using hemagglutination inhibition (HI) assays with reference antiserum raised against vaccine strains A/Darwin/9/2021(H3N2) and A/Victoria/4897/2022(H1pdm) (Fig. 5A). For the A/H3N2 subtype, HI titers against tested strains ranged from 80

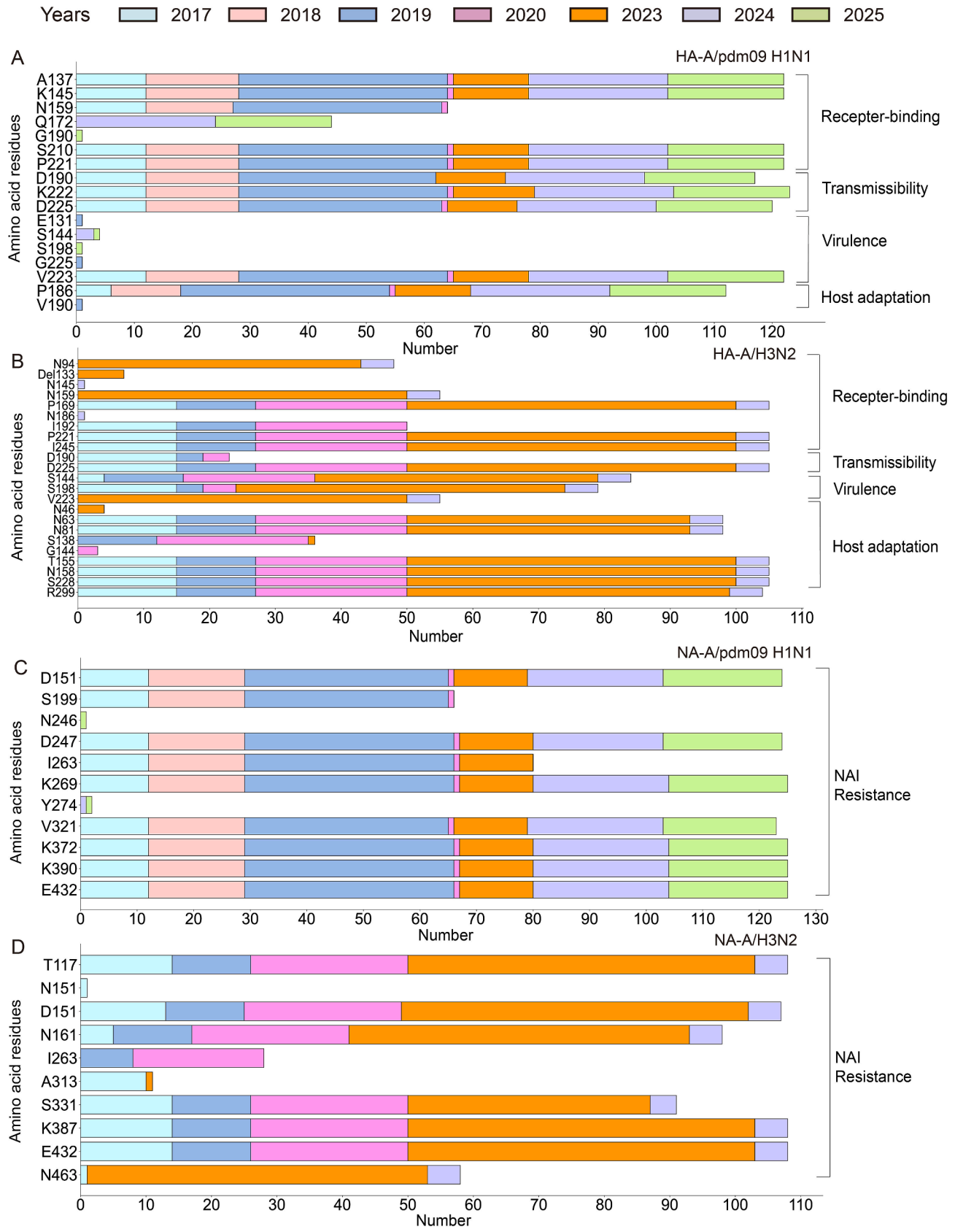

Fig. 4. The risk evaluation of A/pdm09 H1N1 and A/H3N2 isolates in hemagglutinin (HA) and neuraminidase (NA) genes.
A–B. The amino acid residues related to receptor binding, host adaptation, transmissibility, and virulence in H1 (**A**) and H3 segments (**B**). The X-axis refers to the quantity of positive sequences. The Y-axis refers to the amino acid residues in the HA segment (H3 numbering). **C–D.** The amino acid residues related to drug resistance in N1 (**C**) and N2 (**D**) segments. The X-axis refers to the quantity of positive sequences. The Y-axis refers to the amino acid residues in the NA segment (N2 numbering).

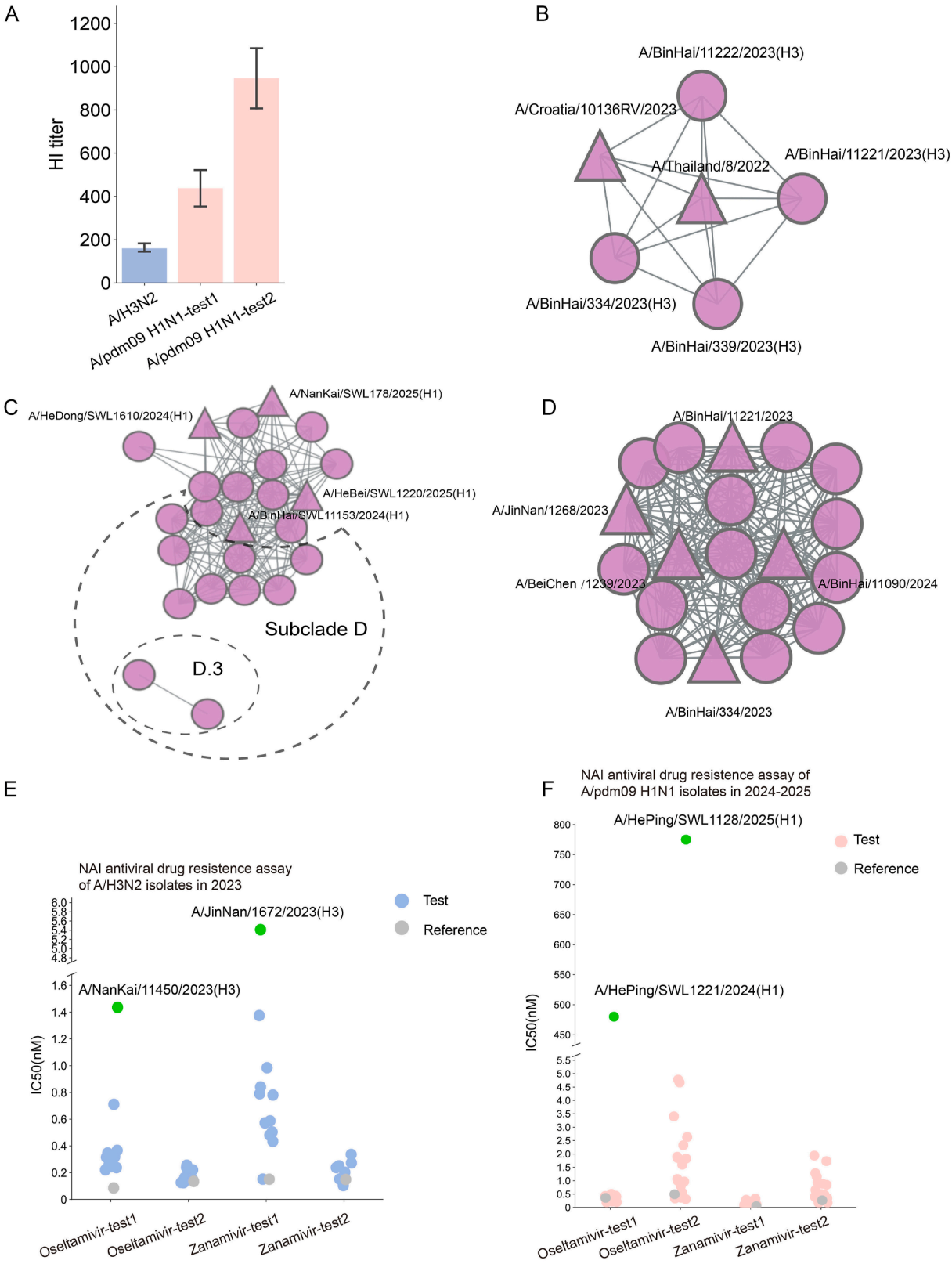

(caption on next page)

Fig. 5. The HA antigenicity and resistance to NAI antiviral drugs in the A/H3N2 and A/pdm09 H1N1 strains.
A. The reactivity of A/H3N2 and A/pdm09 H1N1 in hemagglutination inhibition (HI) assay with reference antiserum raised against the vaccine strain. The HI titers of 21 isolates were detected in the A/H3N2 test (Supplementary Table S4). The HI titers of 19 isolates from 2024 were detected in the A/pdm09 H1N1 test 1 and 22 isolates from 2025 in test 2 (Supplementary Table S5). The X-axis refers to each test. The Y-axis refers to the HI titer against each strain. The bars indicate the mean HI titer against each strain, and the error bars indicate the 95% confidence interval (CI). **B.** The antigenic correlation network between reference strains in Tianjin and A/H3N2 vaccine strains in the Northern Hemisphere influenza season. Nodes in the circle refer to the reference strains in Tianjin, while nodes in the triangle refer to the vaccine strains. A line connecting two nodes means that these nodes are predicted to be antigenically similar. **C–D.** The antigenic correlation network between reference strains in Tianjin and globally circulating subclades in recent years for A/pdm09 H1N1 subtype (**C**) and A/H3N2 subtype (**D**). Nodes in the triangle refer to the reference strains in Tianjin, while circle nodes refer to the global subclades. A line connecting two nodes means that these nodes are predicted to be antigenically similar. **E–F.** The half maximal inhibitory concentration (IC_{50}) of neuraminidase inhibitor (NAI) antiviral drug resistance against A/H3N2 (**E**) and A/pdm09 H1N1 (**F**). The IC_{50} of 12 isolates were detected in the A/H3N2 test 1 and 7 isolates in test 2 (Supplementary Table S6). The IC_{50} of 19 isolates from 2024 were tested in the A/pdm09 H1N1 test 1 and 22 isolates from 2025 in test 2 (Supplementary Table S7). The X-axis refers to each test. The Y-axis refers to the IC_{50} of NAI drugs against each strain. The reference strains were highlighted in gray. The strains with reduced sensitivity to NAI antiviral drug were highlighted in green. The strains without reduced sensitivity to NAI antiviral drug were labeled in blue and pink.

to 320 ($HI_{reference} = 320$). For the A/pdm09 H1N1 subtype, HI titers ranged from 160 to 640 in test 1 ($HI_{reference} = 640$) and 640 to 1280 in test 2 ($HI_{reference} = 1280$) (Supplementary Tables S4 and S5). Due to the update of A/H3N2 vaccine strains for the Northern Hemisphere influenza season, the vaccine strains in 2024–2025 (A/Thailand/8/2022) and 2025–2026 (A/Croatia/10136RV/2023) were selected to analyze antigenic similarity using HA protein sequence-based antigenic correlation networks. Additionally, we selected four A/H3N2 strains that exhibited low and medium HI titers in our assays. As shown in Fig. 5B, antigenic similarity was confirmed between the circulating A/H3N2 and vaccine strains. These results suggest that no antigenic variation or vaccine mismatch occurred in Tianjin.

In our study, the A/pdm09 H1N1 subclades collected during the 2024–2025 mainly belonged to the 6B.1A.5a.2a clade, including the C.1.9 and C.1.9.3 subclades. We selected four reference strains from these subclades and analyzed their antigenicity compared with globally prevalent strains. In the antigenic correlation network, the Tianjin reference strains exhibited antigenic similarity to circulating subclades in other regions, including the C.1.8, C.1.9, C.1.9.1, and C.1.9.3 subclades (Fig. 5C). Meanwhile, we found their antigenic similarity to the D subclade of the 6B.1A.5a.2a.1 clade, which has co-circulated globally after COVID-19, excluding the D.3 subclade. For the A/H3N2 subtype, antigenic similarity was observed between reference strains and globally circulating subclades in recent years, such as the J.2, J.2.1, and J.2.2 subclades (Fig. 5D). Our results demonstrate both antigenic stability and variation in global evolutionary trends during recent influenza seasons.

Next, we evaluated NAI resistance in these isolates. A strain was considered to have low sensitivity when its half maximal inhibitory concentration (IC_{50}) exceeded 10 times that of the reference strain. We found one strain isolated in November 2023 (A/NanKai/11450/2023) exhibited low sensitivity to oseltamivir, and another strain isolated in November 2023 (A/JinNan/1672/2023) showed low sensitivity to zanamivir (Fig. 5E). For the A/pdm09 H1N1 subtype, we found that one strain isolated in 2024 (A/HePing/SWL1221/2024) and another isolated in 2025 (A/HePing/SWL1128/2025) exhibited markedly reduced sensitivity to oseltamivir (Fig. 5F). Notably, the H274Y substitution in the NA gene, which is associated with high-level oseltamivir resistance, was only detected in these two strains in our study (Fig. 4C). All other strains tested were sensitive to both oseltamivir and zanamivir (Supplementary Tables S6 and S7).

DISCUSSION

Seasonal influenza epidemics remain a major global public health concern. In this study, we characterized the epidemic pattern and genomic characteristics of IAV surveillance conducted in Tianjin between 2017 and 2025. We observed regular IAV infection peaks during annual epidemic seasons, except in 2020 and 2021. Phylogenetic analysis revealed distinct IAV clade variations and temporal evolution patterns from 2017 to 2025. Amino acid residues in the HA region associated with human adaptation, transmissibility, receptor-binding affinity, and virulence were identified and showed temporal specificity. Potential reduced sensitivity to NAI antiviral drugs was identified through genomic screening and NAI resistance assays. Furthermore, antigenic similarity was demonstrated between currently circulating strains and vaccine strains.

The epidemiology of seasonal influenza viruses informs surveillance, intervention, and vaccination strategy design (Chen et al., 2024). Globally, A/pdm09 H1N1 virus detection rates showed winter peaks from 2017 to 2024, with the exception of 2020 and 2021. The A/H3N2 subtype exhibited a similar trend but with an additional peak between winter 2021 and the mid-2022 (Chen et al., 2024). Our dynamic surveillance data demonstrated globally consistent IAV transmission patterns in Tianjin. The absence of influenza seasons in 2020 and 2021 was partially attributable to COVID-19 pandemic control measures implemented between April 2020 and April 2023. These non-pharmaceutical interventions (NPIs) comprised entry and exit restrictions, social distancing, mask-wearing, sterilization, and enhanced public hygiene measures (Dhanasekaran et al., 2022). These measures disrupted influenza transmission and led to historically low seasonal influenza activity (Olsen et al., 2020; Dhanasekaran et al., 2022). Given that SARS-CoV-2 and influenza viruses share similar transmission routes, coinfection may exacerbate disease severity in susceptible populations (Huang et al., 2025). This effect was confirmed in Egypt and Missouri (Fahim et al., 2022; Tang et al., 2022). Coinfections were associated with increased viral loads, immune cell infiltration, and elevated inflammatory cytokine levels. Meanwhile, severe lymphocytopenia, reduced antibody levels, and impaired $CD4^+$ T cell responses were observed during coinfection (Bai et al., 2021; Kim et al., 2022). Therefore, the complex epidemiological features of influenza and other respiratory viruses highlighted the importance of dynamic surveillance and comprehensive testing strategies to better understand and prevent respiratory virus coinfections (Huang et al., 2025). Notably, A/pdm09 H1N1 detection rates exceeded A/H3N2 rates during the winters of 2018, 2019, and 2023, while the opposite pattern occurred in 2017 and 2022 globally (Chen et al., 2024). However, Tianjin exhibited some divergent subtype dominance patterns in some years. For example, A/pdm09 H1N1 predominated in winter 2017, whereas A/H3N2 dominated in winters of 2019 and 2023. These regional variations highlight the need for dynamic surveillance of circulating subtypes. Furthermore, age-related influenza infection risks has been reported in Eastern China (Huo et al., 2022). In our study, A/pdm09 H1N1 was more prevalent among infants (0–4 years) and elderly (≥ 65 years), while A/H3N2 predominated in school-aged children (5–14 years). An effective influenza surveillance network can identify circulating subtypes and guide protection of vulnerable populations.

Time-scaled phylogenetic analyses revealed the temporal evolutionary dynamics of IAV lineages. Recent studies have reported a reduction in seasonal influenza virus diversity during the COVID-19 pandemic, with genetic diversity beginning to accumulate again during the post-pandemic transition period (Dhanasekaran et al., 2022; Chen et al., 2024). In our study, we also observed higher genetic diversity in the pre-pandemic period for both A/pdm09 H1N1 and A/H3N2 subtypes as well. The implementation of public health strategies during COVID-19 likely affected seasonal influenza virus

circulation and evolution, leading to fewer dominant lineage in the post-pandemic period. However, the discontinuation of NPIs and the immunity gap in the post-pandemic era prompted further divergence of spatially separated IAV lineages. These distinct lineages may evolve, compete, and potentially circulate more widely (Dhanasekaran et al., 2022; Conroy, 2023). Therefore, long-term genomic surveillance is needed to monitor the dynamic molecular evolution of seasonal influenza A lineages across different regions.

HA is the major envelope glycoprotein for IAV viral entry and thus plays an important role in determining host specificity (Mo et al., 2022). We analyzed H1 and H3 sequences and identified amino acid residues associated with receptor binding and host adaptation, such as Asp225, Pro221, and Asn159, etc. These markers have been linked to enhanced binding affinity to α2,6-SA in avian influenza viruses (Wang et al., 2010; Behera et al., 2016; De Vries et al., 2017). In addition to human influenza virus, the genomic surveillance of animal influenza viruses can track host adaptation mutations to provide early warnings of potential interspecies transmission. Moreover, we identified virulence-enhancing markers, such as Pro186 in the H1 segment (Xing et al., 2021). Notably, some amino acid residues showed temporal specificity, particularly in post-pandemic isolates. Continuous genomic surveillance tracks amino acid substitutions in evolution and dominant lineage shifts over time. Furthermore, antigenicity analysis provides another approach for monitoring IAV antigen variants. Our analyses revealed HA antigen similarity between the vaccine strains and recent isolates, suggesting no current antigenic variation or vaccine mismatch in Tianjin. However, this local antigenic stability may not represent global trends. For example, Tianjin reference strains showed antigenic similarity with some circulating subclades but differed from others, particularly the D.3 subclade. Therefore, dynamic antigenic analysis is essential for tracking global variations and selecting optimal vaccine strains.

NAI antiviral drugs, such as oseltamivir and zanamivir, are extensively used to treat seasonal influenza infections. Several NA amino acid substitutions (e.g., H274Y) in IAV have been associated with reduced drug sensitivity (Chon et al., 2024). The H274Y substitution was first detected in Europe in seasonal A (H1N1) viruses during 2007–2008 and subsequently spread globally (Kawai et al., 2009). While oseltamivir-susceptible A/pdm09 H1N1 viruses later became predominant, the resistant variant reappeared in A/pdm09 H1N1-infected patients both with and without oseltamivir treatment history, as reported in Australia and Japan (Garten et al., 2009; Hurt et al., 2011; Takashita et al., 2015). Furthermore, oseltamivir-resistant influenza A/pdm09 H1N1 viruses have demonstrated community transmission capability even without drug-selective pressure (Lackenby et al., 2011). Consistent with these reports, this substitution in A/pdm09 H1N1 strains in our study exhibited significantly reduced sensitivity to oseltamivir. However, most recent strains remain sensitive to NAI antiviral drugs. Due to difference in experimental methods, more in-depth research *in vivo* and *in vitro* studies are required to elucidate the relationship between amino acid substitution and drug resistance.

Our study has several limitations. First, the sequenced genome coverage was limited. Expanded genomic surveillance with larger sample sizes study is needed to better characterize genetic diversity and viral evolution. Moreover, region-specific amino acid residues associated with viral properties and drug resistance require further validation. Second, our analysis primarily focused on HA and NA genes because of incomplete sequence assembly for other segments. Including other segments, such as PA and M genes, would enable evaluation of reassortment events and resistance to additional drugs like baloxavir. Third, comprehensive *in vitro* studies are needed to investigate viral transmissibility and virulence mechanisms.

CONCLUSIONS

Comprehensive epidemiological and genomic surveillance plays a key role in understanding the molecular characteristics and evolution dynamics of seasonal influenza viruses. Our study characterized the epidemic pattern of IAV in Tianjin from 2017 to 2025 and conducted risk assessments based on genomic analysis. Sustained long-term dynamic surveillance remains essential for monitoring viral evolution across influenza seasons.

MATERIALS AND METHODS

Participants and samples

According to the 2017 National Influenza Surveillance Program of China, we established an influenza surveillance network across 16 districts in Tianjin. From October 2017 to March 2025, we collected 77,473 throat swabs from ILI or SARI patients at 21 sentinel hospitals (Supplementary Table S1). This included 73,536 throat swabs collected from ILI patients, and 3937 throat swabs collected from SARI patients. Influenza-like illness was defined as fever (body temperature $\geq$ 38.0 °C) accompanied by cough or sore throat. Severe acute respiratory infection was defined as hospitalized patients presenting with acute fever (body temperature $\geq$ 38.0 °C) and cough within 48 h of symptom onset, with illness duration under 10 days. All the throat swabs were first tested for influenza virus within 48 h of collection. IAV-positive samples were subsequently subtyped as A/pdm09 H1N1 or A/H3N2 using real-time quantitative PCR.

Isolation of A/pdm09 H1N1 and A/H3N2 viruses

The IAV-positive throat swabs were filtered using a 0.22 μm pore-size filter membrane. A 200 μL aliquot of the filtrate was inoculated onto Madin-Darby canine kidney (MDCK, Chinese National Influenza Center) cells which had been washed twice with 1 mL of Hank's balanced salt solution. Virus adsorption was performed at 37 °C in 5% CO_2 for 1 h, after which unbound virus particles were removed by washing. The cells were then maintained in 1 mL Dulbecco's modified Eagle medium (DMEM, Gibco, U.S.) and 1% L-1-tosylamide-2-phenylethyl chloromethyl ketone (TPCK)-treated trypsin (Sigma-Aldrich, U.S.). Cytopathic effects (CPE) were observed 5 days post-infection using a laser scanning confocal microscope (Zeiss LSM 800, Germany). The virus was harvested and stored at −80 °C.

Sequencing of hemagglutinin (HA) and neuraminidase (NA) segments

Viral nucleic acids were extracted from 50 μL of viral culture fluid using an automatic nucleic acid extraction system (Tianlong; China). The IAV genome was captured using a primer set designed by the Chinese National Influenza Center (Primer A: 5′-GGGGGGAGCAAAAGCAGG-3′; Primer B: 5′-GGGGGGAGCGAAAGCAGG-3′; Primer C: 5′-CGGGTTATTAGTAGAAACAAGG-3′). RT-PCR was performed using the SuperScriptTM III One-Step RT-PCR System with PlatinumTM Taq High Fidelity DNA Polymerase (Invitrogen; U.S.). The amplification protocol consisted of: 45 °C, 1 h; 94 °C, 2 min; 5 × (94 °C, 30 s; 44 °C, 30 s; 68 °C, 3 min); 31 × (94 °C, 30 s; 57 °C, 30 s; 68 °C, 3 min), 68 °C, 7 min.

DNA libraries were prepared using the Nextera XT DNA Library Preparation Kit (Illumina, Inc., U.S.), and library concentration was quantified using a Qubit Fluorometer (Invitrogen, U.S.). Paired-end sequencing was conducted on an Illumina NextSeq 2000 System

(Illumina, Inc., U.S.) following the manufacturer's protocol. Raw sequence data were processed by removing low-quality reads, followed by genome assembly using the MicroFuture Pathogen Microbial Bioinformation Analysis System v1.0.4.9 (MicroFuture; China).

Genomic analysis of A/pdm09 H1N1 and A/H3N2 viruses

We constructed time-scaled phylogenies using BEAST v10.5.0 (Suchard et al., 2018). Reference sequences were obtained from BLAST (Altschul et al., 1990) and GISAID (Khare et al., 2021) databases. Phylogenetic analyses employed a random starting tree with the GTR nucleotide substitution model incorporating estimated base frequencies. A Gamma-distributed (+ Invariant Sites) site heterogeneity model was applied. We implemented an uncorrelated relaxed molecular clock with exponential rate distribution. The Markov chain Monte Carlo analysis was performed with 100 million chain length, yielding Effective Sample Size (ESS) values of 397.7 (A/pdm09 H1N1) and 774.7 (A/H3N2). Tree summarization was conducted using TreeAnnotator v10.5.0, and trees were visualized in FigTree v1.4.4. Viral clades of A/pdm09 H1N1 and A/H3N2 subtypes were annotated using Nextclade v3.10.0 (Aksamentov et al., 2021) (Supplementary Tables S8 and S9).

The risk of host adaptation, transmissibility, virulence, and drug resistance was evaluated using HA and NA sequences on the FluRisk website (http://www.computationalbiology.cn/FluRisk/#/). Antigenic similarity was predicted based on a computational model for HA protein sequences using PREDAV-FluA (Peng et al., 2017) (Supplementary Tables S10-12). For each virus pair, 17 feature variables were derived from HA1 sequences to calculate the odds ratio representing antigenic variation extent. An odds ratio < 1 indicated antigenic similarity between viruses.

Hemagglutination inhibition (HI) assay and NAI antiviral drug resistance assay

For the A/H3N2 virus, the hemagglutination assay was first performed. 100 μL of virus suspension was serially diluted in phosphate buffer saline (PBS). Then, 50 μL of 1% guinea pig red blood cells (RBC) was added to 96-well plates, which were thoroughly mixed. After 1 h incubation at room temperature, the HA titer was determined as the highest dilution showing complete erythrocyte agglutination. Based on the HA titer, viruses were diluted to contain eight units of hemagglutination in 50 μL for subsequent HI assay.

The HI assay was performed to evaluate viral HA antigenicity. Antisera against the vaccine strains A/Darwin/9/2021(H3N2) and A/Victoria/4897/2022/(H1pdm) were selected as references. In brief, 25 μL of serially diluted serum was mixed with 25 μL of diluted virus. 25 μL of reference HA protein served as the positive control, while 25 μL PBS functioned as the negative control. After thorough mixing and 30 min incubation at room temperature, 50 μL of 1% guinea pig RBC was added. Following 1 h incubation, the HI titer was recorded as the highest serum dilution that completely inhibits hemagglutination. Antigenic similarity was defined when the viral HI titer was higher than 1/8 of the reference strain titer.

For the NAI antiviral drug resistance assay, NAI-sensitive strains (A/Pennsylvania/46/2015 and A/Illinois/45/2019) were selected as references. Viral NA activity was first quantified using the NA-Fluor™ Influenza Neuraminidase Assay Kit (Applied Biosystems, Foster City, CA). According to the instrumental signal value and NA activity, the viral suspension was adjusted to achieve equivalent fluorescence intensity. Serial semi-log dilutions of 50 μM oseltamivir (Hoffman-La Roche, Basel, Switzerland) or zanamivir (GlaxoSmithKline, Uxbridge, UK) were prepared in 1 × NA-Fluor™ buffer. Then, 25 μL of diluted NAI solution was combined with 25 μL of diluted virus solution in 96-well plates. 1 × NA-Fluor™ buffer was used as the negative control. After thorough mixing, the reaction mixtures were incubated at 37 °C for 45 min. Next, 50 μL of 2 × NA-Fluor™ substrate working solution was added, followed by incubation at 37 °C for 1 h. 100 μL of NA-Fluor™ substrate stop solution was added, and the fluorescence intensity was measured with a multimode microplate reader (Tecan Trading AG, Switzerland). IC_{50} was determined using GraphPad Prism 5, applying the "log (inhibitor) vs. normalized response–Variable slope" model. The IC_{50} of the reference strain should be within the mean $IC_{50} \pm 3$ standard deviations of strains in each assay.

Statistical analysis

The chi-square tests were performed using GraphPad Prism 9, with the probability of type I error (α) set at 0.05. All figures were created using Adobe Illustrator 2023 (Adobe, California, USA), Python 3.9 packages Matplotlib v3.7.1, and Servier Medical ART (https://smart.servier.com). HI assays and NAI antiviral drug resistance assays were performed once for each strain during our surveillance.

DATA AVAILABILITY

The data of this study are available in the supplementary materials. Sequences are uploaded to Science Data Bank (https://doi.org/10.57760/sciencedb.23954. https://doi.org/10.57760/sciencedb.23954.) that are available from the corresponding author upon reasonable request and with the permission of the institution.

ETHICS STATEMENT

This study was approved by the Ethical Review Board of Tianjin Centers for Disease Control and Prevention (TJCDC-R-2022-017).

AUTHOR CONTRIBUTIONS

Xiaoyan Li: funding acquisition, conceptualization, and methodology, supervision, writing-reviewing and editing. Mingkun Wu: conceptualization, investigation, data curation, validation, formal analysis, software, visualization, and writing-original draft preparation. Liru Guo: investigation, validation, writing-reviewing and editing. Mei Kong: investigation and validation. Ming Zou: investigation, data curation, and validation. Xiaochang Liu: investigation and validation. All authors have read and approved the final manuscript.

CONFLICT OF INTEREST

The authors have declared that no competing interests exist.

ACKNOWLEDGMENTS

We would like to thank the Centers for Disease Control and Prevention in 16 districts and all staff in Tianjin influenza surveillance network laboratories. This study was supported by Tianjin Municipal Health Commission (TJWJ2022ZD010) and Tianjin Key Medical Discipline (Specialty) Construction Project.

APPENDIX A. SUPPLEMENTARY DATA

Supplementary data to this article can be found online at https://doi.org/10.1016/j.virs.2025.07.011.

REFERENCES

Aksamentov, I., Roemer, C., Hodcroft, E., Neher, R., 2021. Nextclade: clade assignment, mutation calling and quality control for viral genomes. J. Open Source Softw. 6, 3773.

Altschul, S.F., Gish, W., Miller, W., Myers, E.W., Lipman, D.J., 1990. Basic local alignment search tool. J. Mol. Biol. 215, 403–410.

An, S.H., Lee, C.Y., Hong, S.M., Song, C.S., Kim, J.H., Kwon, H.J., 2019. Novel mutations evading Avian immunity around the receptor binding site of the clade 2.3.2.1c Hemagglutinin gene reduce viral thermostability and Mammalian pathogenicity. Viruses 11, 923.

Andreev, K., Jones, J.C., Seiler, P., Kandeil, A., Webby, R.J., Govorkova, E.A., 2024. Genotypic and phenotypic susceptibility of emerging avian influenza A viruses to neuraminidase and cap-dependent endonuclease inhibitors. Antivir. Res. 229, 105959.

Bai, L., Zhao, Y., Dong, J., Liang, S., Guo, M., Liu, X., Wang, X., Huang, Z., Sun, X., Zhang, Z., et al., 2021. Coinfection with influenza A virus enhances SARS-CoV-2 infectivity. Cell Res. 31, 395–403.

Behera, A.K., Chandra, I., Cherian, S.S., 2016. Molecular dynamics simulation of the effects of single (S221P) and double (S221P and K216E) mutations in the hemagglutinin protein of influenza A H5N1 virus: a study on host receptor specificity. J. Biomol. Struct. Dyn. 34, 2054–2067.

Boivin, G., 2013. Detection and management of antiviral resistance for influenza viruses. Influenza Other Respir Viruses 7 (Suppl. 3), 18–23.

Boltz, D.A., Douangngeun, B., Phommachanh, P., Sinthasak, S., Mondry, R., Obert, C., Seiler, P., Keating, R., Suzuki, Y., Hiramatsu, H., Govorkova, E.A., Webster, R.G., 2010. Emergence of H5N1 avian influenza viruses with reduced sensitivity to neuraminidase inhibitors and novel reassortants in Lao People'S Democratic Republic. J. Gen. Virol. 91, 949–959.

Butler, J., Hooper, K.A., Petrie, S., Lee, R., Maurer-Stroh, S., Reh, L., Guarnaccia, T., Baas, C., Xue, L., Vitesnik, S., Leang, S.K., Mcvernon, J., Kelso, A., Barr, I.G., Mccaw, J.M., Bloom, J.D., Hurt, A.C., 2014. Estimating the fitness advantage conferred by permissive neuraminidase mutations in recent oseltamivir-resistant A (H1N1)pdm09 influenza viruses. PLoS Pathog. 10, e1004065.

Chandrasekaran, A., Srinivasan, A., Raman, R., Viswanathan, K., Raguram, S., Tumpey, T.M., Sasisekharan, V., Sasisekharan, R., 2008. Glycan topology determines human adaptation of avian H5N1 virus hemagglutinin. Nat. Biotechnol. 26, 107–113.

Chen, Z., Tsui, J.L., Gutierrez, B., Busch Moreno, S., Du Plessis, L., Deng, X., Cai, J., Bajaj, S., Suchard, M.A., Pybus, O.G., Lemey, P., Kraemer, M.U.G., Yu, H., 2024. COVID-19 pandemic interventions reshaped the global dispersal of seasonal influenza viruses. Science 386, eadq3003.

Chon, I., Win, S.M.K., Phyu, W.W., Saito, R., Kyaw, Y., Win, N.C., Lasham, D.J., Tin, H. H., Tamura, T., Otoguro, T., Wagatsuma, K., Sun, Y., Li, J., Watanabe, H., 2024. Whole-genome analysis of the influenza A(H1N1)pdm09 viruses isolated from influenza-like illness outpatients in Myanmar and community-acquired oseltamivir-resistant strains present from 2015 to 2019. Viruses 16, 1300.

Conroy, G., 2023. What's behind China's mysterious wave of childhood pneumonia? Nature. https://doi.org/10.1038/d41586-023-03732-w.

De Vries, R.P., Tzarum, N., Peng, W., Thompson, A.J., Ambepitiya Wickramasinghe, I.N., De La Pena, A.T.T., Van Breemen, M.J., Bouwman, K.M., Zhu, X., Mcbride, R., Yu, W., Sanders, R.W., Verheije, M.H., Wilson, I.A., Paulson, J.C., 2017. A single mutation in Taiwanese H6N1 influenza hemagglutinin switches binding to human-type receptors. EMBO Mol. Med. 9, 1314–1325.

Dhanasekaran, V., Sullivan, S., Edwards, K.M., Xie, R., Khvorov, A., Valkenburg, S. A., Cowling, B.J., Barr, I.G., 2022. Human seasonal influenza under COVID-19 and the potential consequences of influenza lineage elimination. Nat. Commun. 13, 1721.

Fahim, M., Roshdy, W.H., Deghedy, O., Kamel, R., Naguib, A., Showky, S., Elguindy, N., Abdel Fattah, M., Afifi, S., Mohsen, A., Kandeel, A., Abdelghaffar, K., 2022. Epidemiology, disease severity and outcome of severe acute respiratory syndrome coronavirus 2 and influenza viruses coinfection seen at Egypt integrated acute respiratory infections surveillance, 2020-2022. Can. J. Infect. Dis. Med. Microbiol. 2022, 7497500.

Gamblin, S.J., Skehel, J.J., 2010. Influenza hemagglutinin and neuraminidase membrane glycoproteins. J. Biol. Chem. 285, 28403–28409.

Garten, R.J., Davis, C.T., Russell, C.A., Shu, B., Lindstrom, S., Balish, A., Sessions, W.M., Xu, X., Skepner, E., Deyde, V., et al., 2009. Antigenic and genetic characteristics of swine-origin 2009 A(H1N1) influenza viruses circulating in humans. Science 325, 197–201.

Huang, Y., Li, S., Ye, W., Wang, H., Su, J., Gao, L., Shi, R., Mou, X., Leng, S.X., Xiao, C., Chen, G., 2025. Viral infections in elderly individuals: a comprehensive overview of SARS-CoV-2 and influenza susceptibility, pathogenesis, and clinical treatment strategies. Vaccines (Basel) 13, 431.

Huo, X., Fu, J., Dai, Q., Zhu, F., 2022. Influenza virus subtype/lineage-specific seasonal patterns and age-related infection risk, in Eastern China. J. Infect Dev Ctries. 16, 1928–1932.

Hurt, A.C., Hardie, K., Wilson, N.J., Deng, Y.M., Osbourn, M., Gehrig, N., Kelso, A., 2011. Community transmission of oseltamivir-resistant A(H1N1)pdm09 influenza. N. Engl. J. Med. 365, 2541–2542.

Imai, M., Watanabe, T., Hatta, M., Das, S.C., Ozawa, M., Shinya, K., Zhong, G., Hanson, A., Katsura, H., Watanabe, S., Li, C., Kawakami, E., Yamada, S., Kiso, M., Suzuki, Y., Maher, E.A., Neumann, G., Kawaoka, Y., 2012. Experimental adaptation of an influenza H5 HA confers respiratory droplet transmission to a reassortant H5 HA/H1N1 virus in ferrets. Nature 486, 420–428.

Jayaraman, A., Pappas, C., Raman, R., Belser, J.A., Viswanathan, K., Shriver, Z., Tumpey, T.M., Sasisekharan, R., 2011. A single base-pair change in 2009 H1N1 hemagglutinin increases human receptor affinity and leads to efficient airborne viral transmission in ferrets. PLoS One 6, e17616.

Kawai, N., Ikematsu, H., Iwaki, N., Kondou, K., Hirotsu, N., Kawashima, T., Maeda, T., Tanaka, O., Doniwa, K., Kashiwagi, S., 2009. Clinical effectiveness of oseltamivir for influenza A(H1N1) virus with H274Y neuraminidase mutation. J. Infect. 59, 207–212.

Khare, S., Gurry, C., Freitas, L., Schultz, M.B., Bach, G., Diallo, A., Akite, N., Ho, J., Lee, R.T., Yeo, W., Curation Team, G.C., Maurer-Stroh, S., 2021. GISAID's role in pandemic response. China CDC Wkly 3, 1049–1051.

Kim, E.H., Nguyen, T.Q., Casel, M.a.B., Rollon, R., Kim, S.M., Kim, Y.I., Yu, K.M., Jang, S. G., Yang, J., Poo, H., Jung, J.U., Choi, Y.K., 2022. Coinfection with SARS-CoV-2 and influenza A virus increases disease severity and impairs neutralizing antibody and CD4(+) T cell responses. J. Virol. 96, e0187321.

Krammer, F., Smith, G.J.D., Fouchier, R.a.M., Peiris, M., Kedzierska, K., Doherty, P.C., Palese, P., Shaw, M.L., Treanor, J., Webster, R.G., García-Sastre, A., 2018. Influenza. Nat. Rev. Dis. Primers 4, 3.

Lackenby, A., Moran Gilad, J., Pebody, R., Miah, S., Calatayud, L., Bolotin, S., Vipond, I., Muir, P., Guiver, M., Mcmenamin, J., Reynolds, A., Moore, C., Gunson, R., Thompson, C., Galiano, M., Bermingham, A., Ellis, J., Zambon, M., 2011. Continued emergence and changing epidemiology of oseltamivir-resistant influenza A(H1N1) 2009 virus, United Kingdom, winter 2010/11. Euro Surveill 16, 19784.

Lee, A.J., Carson, S., Reyne, M.I., Marshall, A., Moody, D., Allen, D.M., Allingham, P., Levickas, A., Fitzgerald, A., Bell, S.H., et al., 2024. Wastewater monitoring of human and avian influenza A viruses in Northern Ireland: a genomic surveillance study. The Lancet. Microbe 5, 100933.

Lee, N., Khalenkov, A.M., Lugovtsev, V.Y., Ireland, D.D., Samsonova, A.P., Bovin, N.V., Donnelly, R.P., Ilyushina, N.A., 2018. The use of plant lectins to regulate H1N1 influenza A virus receptor binding activity. PLoS One 13, e0195525.

Li, X., Dong, Z., Li, J., Dou, C., Tian, D., Ma, Z., Liu, W., Gao, G.F., Bi, Y., 2024. Genetic characteristics of H1N1 influenza virus outbreak in China in early 2023. Virol Sin. 39, 520–523.

Mo, J.S., Abente, E.J., Cardenas Perez, M., Sutton, T.C., Cowan, B., Ferreri, L.M., Geiger, G., Gauger, P.C., Perez, D.R., Vincent Baker, A.L., Rajao, D.S., 2022. Transmission of human influenza A virus in pigs selects for adaptive mutations on the HA gene. J. Virol. 96, e0148022.

Nair, H., Brooks, W.A., Katz, M., Roca, A., Berkley, J.A., Madhi, S.A., Simmerman, J.M., Gordon, A., Sato, M., Howie, S., et al., 2011. Global burden of respiratory infections due to seasonal influenza in young children: a systematic review and meta-analysis. Lancet 378, 1917–1930.

Nelson, M.I., Viboud, C., Simonsen, L., Bennett, R.T., Griesemer, S.B., St George, K., Taylor, J., Spiro, D.J., Sengamalay, N.A., Ghedin, E., Taubenberger, J.K., Holmes, E. C., 2008. Multiple reassortment events in the evolutionary history of H1N1 influenza A virus since 1918. PLoS Pathog. 4, e1000012.

Olsen, S.J., Azziz-Baumgartner, E., Budd, A.P., Brammer, L., Sullivan, S., Pineda, R.F., Cohen, C., Fry, A.M., 2020. Decreased Influenza Activity during the COVID-19 Pandemic - united States, Australia, Chile, and South Africa, 2020. MMWR Morb. Mortal. Wkly. Rep. 69, 1305–1309.

Peng, Y., Wang, D., Wang, J., Li, K., Tan, Z., Shu, Y., Jiang, T., 2017. A universal computational model for predicting antigenic variants of influenza A virus based on conserved antigenic structures. Sci. Rep. 7, 42051.

Suchard, M.A., Lemey, P., Baele, G., Ayres, D.L., Drummond, A.J., Rambaut, A., 2018. Bayesian phylogenetic and phylodynamic data integration using BEAST 1.10. Virus Evol. 4, vey016.

Takashita, E., Kiso, M., Fujisaki, S., Yokoyama, M., Nakamura, K., Shirakura, M., Sato, H., Odagiri, T., Kawaoka, Y., Tashiro, M., 2015. Characterization of a large cluster of influenza A(H1N1)pdm09 viruses cross-resistant to oseltamivir and peramivir during the 2013-2014 influenza season in Japan. Antimicrob. Agents Chemother. 59, 2607–2617.

Tang, C.Y., Boftsi, M., Staudt, L., Mcelroy, J.A., Li, T., Duong, S., Ohler, A., Ritter, D., Hammer, R., Hang, J., Wan, X.F., 2022. SARS-CoV-2 and influenza co-infection: a cross-sectional study in central Missouri during the 2021-2022 influenza season. Virology 576, 105–110.

Tsou, T.P., Su, C.P., Huang, W.T., Yang, J.R., Liu, M.T., 2017. Influenza A(H3N2) virus variants and patient characteristics during a summer influenza epidemic in Taiwan, 2017. Euro Surveill. 22, 17-00767.

Wagner, R., Matrosovich, M., Klenk, H.D., 2002. Functional balance between haemagglutinin and neuraminidase in influenza virus infections. Rev. Med. Virol. 12, 159–166.

Wang, W., Lu, B., Zhou, H., Suguitan Jr., A.L., Cheng, X., Subbarao, K., Kemble, G., Jin, H., 2010. Glycosylation at 158N of the hemagglutinin protein and receptor binding specificity synergistically affect the antigenicity and immunogenicity of a live attenuated H5N1 A/Vietnam/1203/2004 vaccine virus in ferrets. J. Virol. 84, 6570–6577.

Wedde, M., Biere, B., Wolff, T., Schweiger, B., 2015. Evolution of the hemagglutinin expressed by human influenza A(H1N1)pdm09 and A(H3N2) viruses circulating between 2008-2009 and 2013-2014 in Germany. Int J Med Microbiol 305, 762–775.

Xing, L., Chen, Y., Chen, B., Bu, L., Liu, Y., Zeng, Z., Guan, W., Chen, Q., Lin, Y., Qin, K., Chen, H., Deng, X., Wang, X., Song, W., 2021. Antigenic drift of the hemagglutinin from an influenza A (H1N1) pdm09 clinical isolate increases its pathogenicity in vitro. Virol. Sin. 36, 1220–1227.

Ye, J., Sorrell, E.M., Cai, Y., Shao, H., Xu, K., Pena, L., Hickman, D., Song, H., Angel, M., Medina, R.A., Manicassamy, B., Garcia-Sastre, A., Perez, D.R., 2010. Variations in the hemagglutinin of the 2009 H1N1 pandemic virus: potential for strains with altered virulence phenotype? PLoS Pathog. 6, e1001145.

Zhao, X., Gu, Y., Tang, X., Jiang, C., Fang, F., Chu, W., Tao, L., Zhang, X., Chen, M., Wu, H., Xie, Y., Liu, J., Teng, Z., 2024. Whole-genome analysis of circulating influenza A virus (H3N2) strains in Shanghai, China from 2005 to 2023. Emerg. Microb. Infect. 13, 2396867.